

# Insights on Debris Flow Growth: Collisions and Contractile Skins

C.E. Choi

Department of Civil Engineering, The University of Hong Kong, HKSAR, China

doi: <https://doi.org/10.21467/proceedings.126.3>

## Abstract

Soil bed erosion is perhaps the most important momentum exchange process that governs the growth and destructive potential of landslides, such as debris flow. Existing erosion models only consider shear stresses induced by the basal friction of the flow as the driving mechanism and adopt saturated soil mechanics to describe the failure of the soil bed. However, field observations have hinted at the importance of collisional stresses as a major driving mechanism of erosion and soil beds in nature are rarely saturated when landslides occur. In this plenary paper, unsaturated soil mechanics is used to characterize soil bed erosion by flows dominated by collisional stresses. Experiments were conducted to model the erosion of unsaturated sandy beds with a wide range of initial matric suction, which is a measure of the capillary stresses, by gravel flows. Key findings and their implications to the delineation of debris flow hazards are discussed.

**Keywords:** Debris flow, Physical tests, Unsaturated soil mechanics

## 1 Introduction

Landslides, such as debris flow, travel at high speeds and may cause fatalities and damage to infrastructure in mountainous regions (Froude & Petley 2018; Jakob et al. 2012). The destructive potential of a debris flow hinges on its ability to erode soil bed material along its flow path (Hungr et al. 2005). Therefore, reliable predictions of erosion are crucial when delineating debris flow hazards. Despite a strong foundation of research work on erosion (Cao et al. 2004; Fraccarollo & Capart 2002; McDougall & Hungr 2005; Medina et al. 2008; Pirulli & Pastor 2012; Sovilla et al. 2006; Sutherland 1967; Takahashi 1978), it remains one of the most difficult momentum exchange processes to model and predict (Hungr et al. 2005; Iverson 2012). Reliable predictions of erosion have direct implications on the design capacity of the mitigation measures used to arrest debris flows.

The bulk of existing erosion theories in the literature rely on shear stress induced by the friction at the base of the flow as the driving mechanism (Iverson 2012; Takahashi 1978). However, unique field measurements of natural debris flows taken from Illgraben, Switzerland, show that large boulders at the flow front generate high collisional stresses (McArdell et al. 2007), which may have an even more prominent effect on erosion compared to friction-induced basal shear stress. In fact, field observations show that collisional stresses at the base of a flow may drive erosion by generating point loads as high as 10 MPa (Okuda et al. 1980), which is more than sufficient to cause even bedrock to fail (Stock & Dietrich 2006). Despite the important role played by collisional stresses, the bulk of existing erosion theories for soil beds still focus on friction-induced basal shear stress as the driving mechanism and overlook the effects of basal collisional stresses.

Another common idealization made in existing theoretical models of soil bed erosion is that the strength of soil can be estimated using saturated soil mechanics (Iverson 2012). However, channel



beds are seldom saturated in nature when landslides occur (McCoy et al. 2012). In fact, for unsaturated soils, capillary stresses due to the presence of air-water interfaces significantly contribute to the shear strength (Fredlund et al. 1996; Vanapalli et al. 1996). The peak shear strength of unsaturated soil has been reported to be up to three times larger than that at its saturated state (Fredlund et al. 1996; Vanapalli et al. 1996). Furthermore, in saturated soils, any external undrained loading is directly transferred to the pore water. However, for unsaturated soils, the compressibility of the pore air also plays an important role in the transfer of undrained loading to the soil bed (Skempton 1954). Evidently, considering the capillary stresses in the soil bed is an important step towards the realistic modelling of debris flow erosion and growth in the event that the soil bed is unsaturated.

In this plenary paper, details of a new theory on soil bed erosion based on unsaturated soil mechanics and the assumption that soil bed erosion is driven by collisional stresses are presented. A series of experiments were carried out to evaluate the proposed erosion theory.

## 2 Modified Strength Normalised Collisional Stress for Erosion of Unsaturated Soil Beds

The point loads imposed on a soil bed by a debris flows scale with the collisional stresses  $\sigma_i$ , which is defined by Bagnold (1954) as follows:

$$\sigma_i = v_s \rho_s D_e^2 \dot{\gamma}^2 \quad (1)$$

where  $v_s$  is the solid fraction of the debris flow,  $\rho_s$  is the density of the solid particles,  $D_e$  is the characteristic grain diameter of the solid particles and  $\dot{\gamma}$  is the shear rate near the base of a debris flow. The erosion rate  $\dot{e}$  of a soil bed by collisional stresses is proportional to the strength normalized collisional stress  $N_{SNCS}$ , which is defined as the ratio of the basal collisional stresses to the shear strength of the soil bed  $\tau_f$ :

$$\dot{e} = K \cdot N_{SNCS} \quad (2a)$$

$$N_{SNCS} = \frac{v_s \rho_s D_e^2 \dot{\gamma}^2}{\tau_f} \quad (2b)$$

where  $K$  is a coefficient related to the properties of the flow material and may be interpreted as the ratio of the stresses from point loads imposed on the soil beds to the collisional stresses (Equation 1). Equation 2 was originally proposed to estimate the erosion of bedrock by collisional flows (Stock & Dietrich 2006), where the erosion rate was reported to exhibit a linear relationship with  $N_{SNCS}$ . However, the failure mechanisms for soil and rock are different. For soil beds, failure occurs when the induced shear stress exceeds the shear strength (Terzaghi 1936). After which, soil particles will slide along a failure plane. In contrast, rock beds fail by tensile failure, which is initiated at discontinuities (Jaeger et al. 2009). Thus, the denominator of  $N_{SNCS}$  is modified to cater for unsaturated soils.

For unsaturated soils, the voids and soil skeleton enable capillary action, whereby air-water interfaces called contractile skins act as elastic membranes to hold soil particles together via surface tension (Fredlund et al. 1978). The shear strength of unsaturated soils  $\tau$  can be expressed as follows (Fredlund et al. 1978; Lu 2008):

$$\tau = (\sigma_n - u_a) \tan \phi' + (u_a - u_w) \tan \phi^b \quad (3)$$

where  $\sigma_n$ ,  $u_a$  and  $u_w$  are the normal stress, pore air pressure and pore water pressure, respectively,  $\phi'$

is the internal friction angle of the soil and  $\tan\phi^b$  quantifies the effect of matric suction ( $u_a - u_w$ ) on the shear strength. Equation 3 shows that the shear strength of unsaturated soils is governed by two stress state parameters, specifically the net normal stress ( $\sigma_n - u_a$ ) and the matric suction. Although the shear strength of soil subjected to rapid loading may be rate-dependent, these effects are not considered here for simplicity.

Debris flows impose rapid loading on soil beds (Hung et al. 2014; Takahashi 1978). If the rate of loading is higher than that at which the pore fluid drains from the soil matrix, the loading is considered undrained and pore pressure will increase. The response of the pore air pressure  $\Delta u_a$  and pore water pressure  $\Delta u_w$  to external undrained loading  $\Delta\sigma$  can be calculated as follows (Skempton 1954):

$$\Delta u_a = B_a \cdot \Delta\sigma \quad (4a)$$

$$\Delta u_w = B_w \cdot \Delta\sigma \quad (4b)$$

where  $B_a$  is the pore air pressure parameter and  $B_w$  is the pore water pressure parameter.

In saturated soils, the pore water pressure parameter is assumed to be unity because the compressibility of the pore water is relatively low compared to that of the soil skeleton (Bishop 1954; Hasan & Fredlund 1980; Skempton 1954). However, in unsaturated soils, the high compressibility of the pore air renders increases in both the pore water pressure and pore air pressure smaller than the external loading. For unsaturated soils subjected to undrained loading, the pore pressure parameters can be expressed as follows (Hilf 1948):

$$B_a = B_w = 1 / \left[ 1 + \frac{(1-S_0)n_0}{m_v(u_{a0} + \Delta u_a)} \right] \quad (5)$$

where  $S_0$  is the initial degree of saturation of soil bed,  $n_0$  is the initial void ratio of the soil,  $m_v$  is the compressibility of the soil and  $u_{a0}$  is the initial pore air pressure. If the pore air pressure is assumed to be atmospheric, then the pore pressure during undrained loading can be calculated as follows:

$$u_a = B_a \cdot \Delta\sigma \quad (6a)$$

$$u_w = -(u_a - u_w)_0 + B_w \cdot \Delta\sigma \quad (6b)$$

where  $(u_a - u_w)_0$  is the initial matric suction. Equation 6b can then be used to explain why positive pore water pressure is more readily generated for soil beds with a higher bed water content, as observed by Iverson et al. (2011). The change in the pore pressure during undrained loading results in a change in the shear strength of the unsaturated soil. By substituting Equation 6 into Equation 3, the shear strength of an unsaturated soil bed undergoing undrained loading can be expressed as follows:

$$\tau_f = \sigma_n \tan\phi' + (u_a - u_w)_0 \tan\phi^b - B_a \sigma_n \tan\phi' \quad (7)$$

Equation 7 can then be substituted into Equation 2 to estimate the erosion rate of an unsaturated soil bed subjected to collisional stresses:

$$\dot{e} = K \cdot N_{SNCS} \quad (8a)$$

$$N_{SNCS} = \frac{v_s \rho_s D_e^2 \dot{\gamma}^2}{\sigma_n \tan\phi' + (u_a - u_w)_0 \tan\phi^b - B_a \sigma_n \tan\phi'} \quad (8b)$$

The modified dimensionless number  $N_{\text{SNCS}}$  will be evaluated using the physical experimental data, which will be discussed later in this plenary paper.

### 3 Physical Modelling of Soil Bed Erosion by Collisional Flows

The goal of the erosion experiments was to model a debris flow front, which generally consists of a permeable assembly of coarse grains (Iverson 1997). The viscous stress caused by the interstitial fluid can be neglected compared to the collisional inter-particle stresses generated by the coarse grains at the front of a debris flow (McArdell et al. 2007). The Savage number  $N_{\text{Sav}}$ , which characterizes the relative importance between interparticle collisional and frictional stresses, is the most relevant dimensionless number for scaling the modelling flows:

$$N_{\text{Sav}} = \frac{v_s \rho_s D_e^2 \dot{\gamma}^2}{\rho g h \tan \phi'} \quad (9)$$

The inter-particle collisional stresses dominate the interaction of solid grains when the Savage number  $N_{\text{Sav}}$  is greater than 0.1 (Savage & Hutter 1989). The configuration of the experimental setup was selected based on the aforementioned scaling considerations to ensure the generated flows are dominated by collisional stresses.

The flume model (Fig. 1) used in this study is 2 m in length and 0.2 m in width. The channel bed has a 1.3-m long rigid section, followed by a 0.7-m long erodible section. During each test, a gravel assembly with an initial depth  $h_0$  of 0.48 m and a width  $r_0$  of 0.5 m was prepared in the container. The friction angle for the gravel is  $43.5^\circ$ . The grain size of the gravels used in this study range from 10 mm to 15 mm, with an effective diameter  $D_e$  of 12 mm. The gate lifts vertically and is controlled pneumatically to simulate dam-break initiation of the dry gravel material retained behind the gate (Stansby et al. 1998). Upon dam-break initiation, the mass of gravel was allowed to accelerate down the rigid bed before flowing on top of the erodible one. The erodible bed consists of sandy soil with negligible clay content to represent the channel bed deposits observed in the field (Chen & Lee 2004). The volumetric water content of the erodible bed was varied from 0 to 0.3, corresponding to initial matric suctions from 97.8 kPa to 0.1 kPa. The dry density of the bed material was controlled and only varied by less than 3% for each test. Table 1 shows a summary of the test program. Details of the experimental setup are discussed in Song & Choi (2021).

A pore pressure transducer installed at a depth of 0.12 m in the erodible soil bed along the centerline of the channel and at an inclined distance of 0.4 m downstream from the interface between the non-erodible and erodible beds. A high-speed camera was installed at the side of the flume to capture the flow kinematics. The images captured by a high-speed camera installed at the side of flume. Images from the camera are analyzed with the Particle Image Velocimetry (PIV) technique (Thielicke & Stamhuis 2014) to deduce the velocity field of the flow. An ultrasonic sensor was mounted above the channel bed just before the erodible bed to measure the flow depth. The initial matric suction of the soil bed was measured using a tensiometer. To reveal the erosion depth, 12 erosion columns were installed along the centerline of the erodible section at distances of 0.04 m, 0.08 m, 0.12 m, 0.16 m, 0.20 m, 0.26 m, 0.32 m, 0.38 m, 0.44 m, 0.50 m, 0.56 m and 0.62 m from the interface between the non-erodible and erodible beds (Fig. 2). The washers have inner and outer diameters of 3.1 mm and 7 mm, respectively. The washer columns were prepared before the soil bed was prepared to the same

height as the initial height of the columns. Then, the rods were removed without disturbing the soil and washers. The erosion depth is the difference between the height of the columns before and after each test.

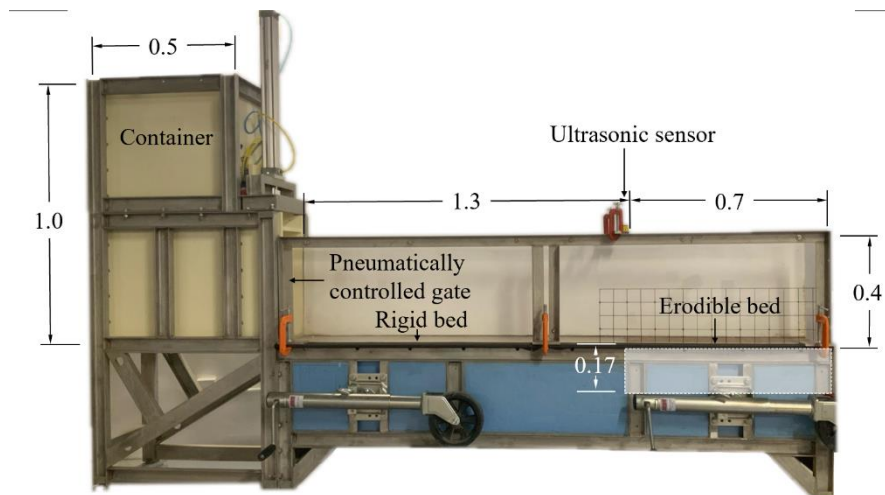


Figure 1: Experimental setup.

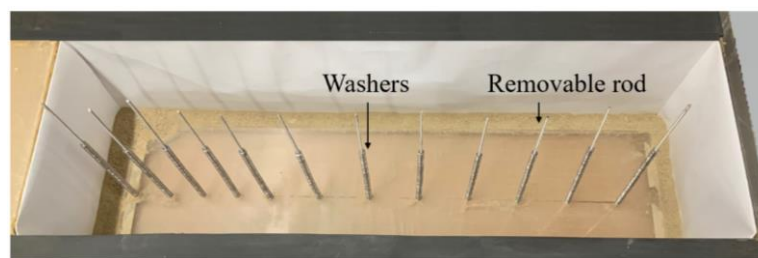
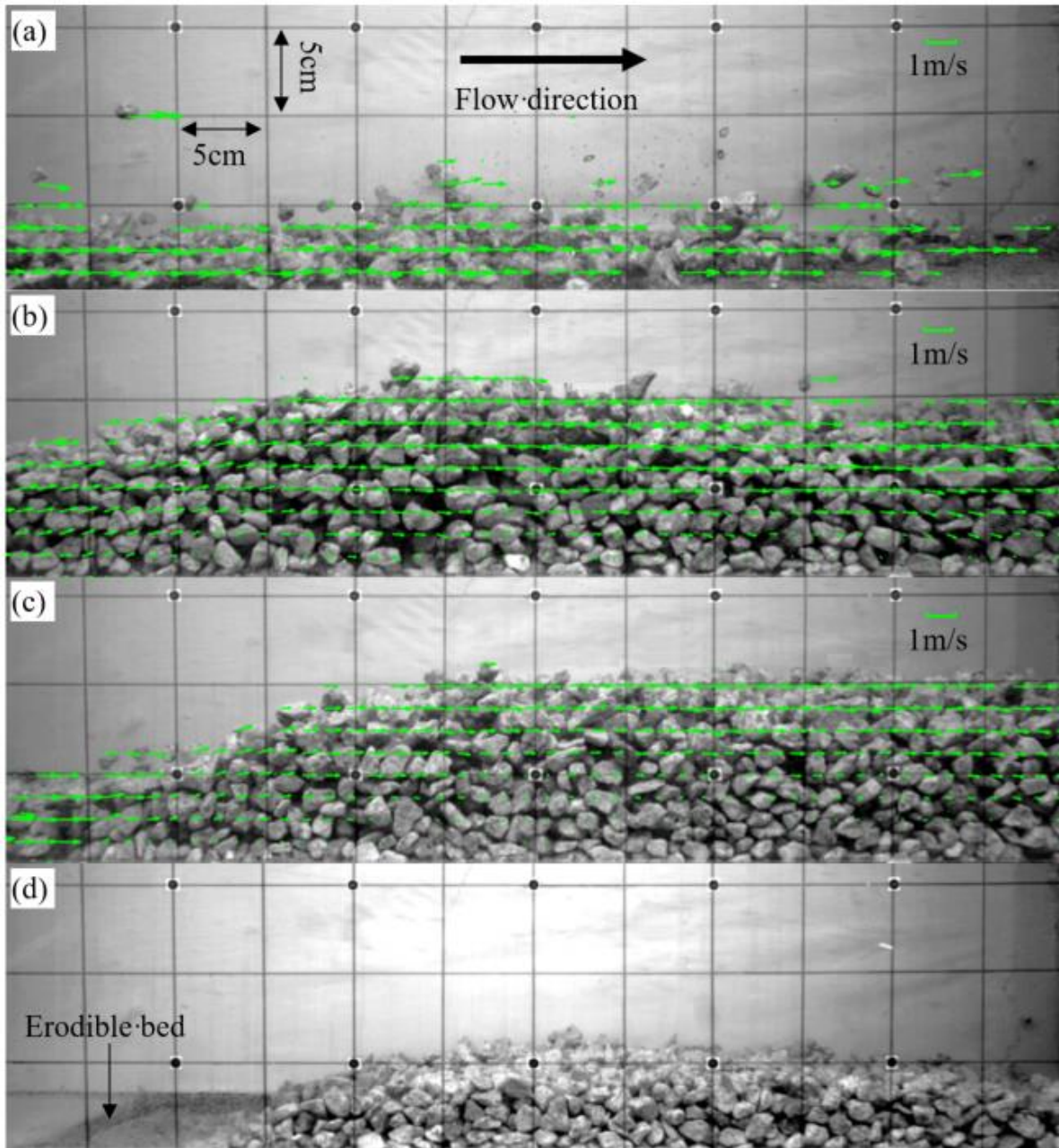


Figure 2: Erosion columns.

Table 1. Summary of test program (Song & Choi 2021)

Test ID	Dry density, $\rho_d$ (kg/m <sup>3</sup> )	Void ratio, $n$	Volumetric water content, $\vartheta$	Initial matric suction, $(u_a - u_w)_0$ (kPa)	Pore pressure parameter, $B$	Shear strength at failure, $\tau_f$ (kPa)
$\vartheta_0$	1305	1.01	0.00	-	0.48	0.62
$\vartheta_{006}$	1307	1.00	0.06	97.8	0.51	1.10
$\vartheta_{011}$	1315	0.99	0.11	79.5	0.54	5.60
$\vartheta_{013}$	1329	0.97	0.13	68.0	0.55	7.38
$\vartheta_{016}$	1319	0.99	0.16	26.0	0.58	6.74
$\vartheta_{018a}$	1319	0.99	0.18	14.0	0.59	4.12
$\vartheta_{018b}$	1310	1.00	0.18	10.8	0.59	3.24
$\vartheta_{020}$	1339	0.96	0.20	5.0	0.60	1.93
$\vartheta_{021}$	1327	0.97	0.21	1.7	0.61	0.95
$\vartheta_{022}$	1329	0.97	0.22	1.3	0.63	0.85
$\vartheta_{024}$	1323	0.98	0.24	0.9	0.64	0.71
$\vartheta_{028}$	1329	0.97	0.28	0.4	0.68	0.53
$\vartheta_{030}$	1340	0.96	0.30	0.1	0.71	0.37



**Figure 3:** Observed flow kinematics captured using the high-speed camera with PIV analysis with a bed volumetric water content  $\vartheta = 0.22$ . (a)  $t = 0.22$  s, flow front passes the erodible bed; (b)  $t = 1.19$  s, deceleration of the flow; (c)  $t = 2.16$  s, deposition of the flow; (d)  $t = 3.14$  s, final deposited profile.

## 4 Interpretation of Results

### 4.1 Erosion Kinematics

Typical kinematics captured by the high-speed camera mounted at the side of the 2-m flume and the corresponding PIV analysis for each snapshot are shown in Fig. 3. The size of the vectors denotes the magnitude of the velocity. Fig. 3a shows the arrival of the dispersed flow front of gravel flow in the field of view. The dispersed flow front was collisional and without sustained contact. The gravel particles at the flow front were observed to collide with the erodible bed and some of the bed material is observed to be picked up into the flow. This indicates that on top of friction induced stresses, collisional stresses in the flow front also play a role in erosion. Erosion occurs without persisting

contacts between gravel particles. This implies that collisional stresses are the dominant grain stress causing erosion at the flow front. Fig. 3b shows the deceleration of the flow, which is accompanied by the gradual increase of the flow height. The motion of the gravel particles exhibits a transition from a gas-like flow to a dense one. The velocity of the gravel particles at the base of the flow gradually decreases. Fig. 3c shows the deposition process, where the velocity of the gravel at the bottom layer of the flow decreases to zero and deposits (Fig. 3d).

#### **4.2 Effects of Matric Suction on Soil Bed Erosion**

Fig. 4 shows the relationship between the average erosion rate, the shear strength of the soil bed at failure, and the initial matric suction of the soil bed. The average erosion rate is calculated by dividing the average erosion depth by the erosion duration estimated from the videos captured by the high-speed camera. The variation in the average erosion rate with initial matric suction exhibits a parabola-like relationship. The average erosion rate decreases with increasing matric suction until a minimum is reached. Afterwards, the average erosion rate increases with the matric suction. However, the variation in the shear strength with the matric suction exhibits an inverted parabola-like relationship. This observation agrees with Equation 2 in that the erosion rate should be inversely related to the shear strength. Iverson et al. (2011) shows that the average erosion depth increases linearly with the bed water content from the large-scale flume experiments. However, a linear trend only tells part of the story. The erosion depth tends to increase with the bed water content when it is higher than a specific value, as shown by the parabola-like relationship proposed in this study (Fig. 5a). The measured data exhibits parabola-like relationship between the average erosion depth and the bed water content. A more comprehensive set of field data reported by McCoy et al. (2012) can be used to validate the proposed parabola-like relationship between the erosion rate and the bed water content (Fig. 5b). The field data was obtained from an observation station at Chalk Cliffs, Colorado, U.S., from September 2009 to June 2011. The field data further corroborates the parabola-like relationship between the average erosion rate and the bed water content. Thus, to improve the fundamental understanding and predictions of soil bed erosion, it is necessary to consider hydro-mechanical coupling.

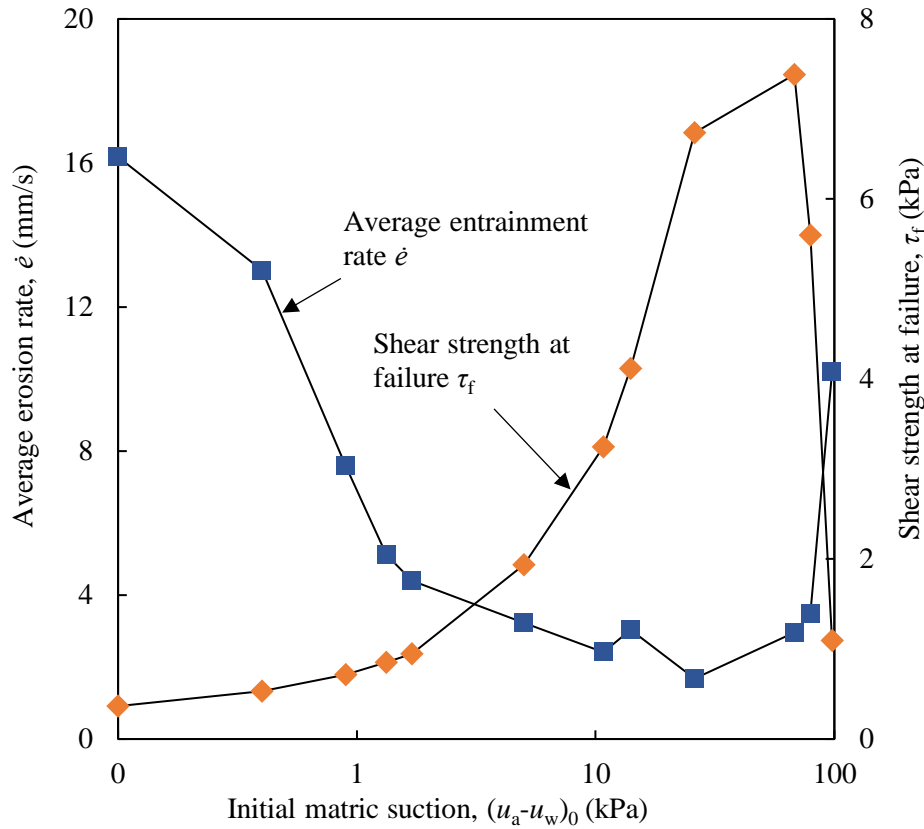


**Figure 4:** Measured erosion rate  $\dot{e}$  and the calculated shear strength of bed material at failure  $\tau_f$  against the measured initial matric suction of the erodible bed  $(u_a - u_w)_0$ . The shear strength at failure  $\tau_f$  is calculated using Equation 7.

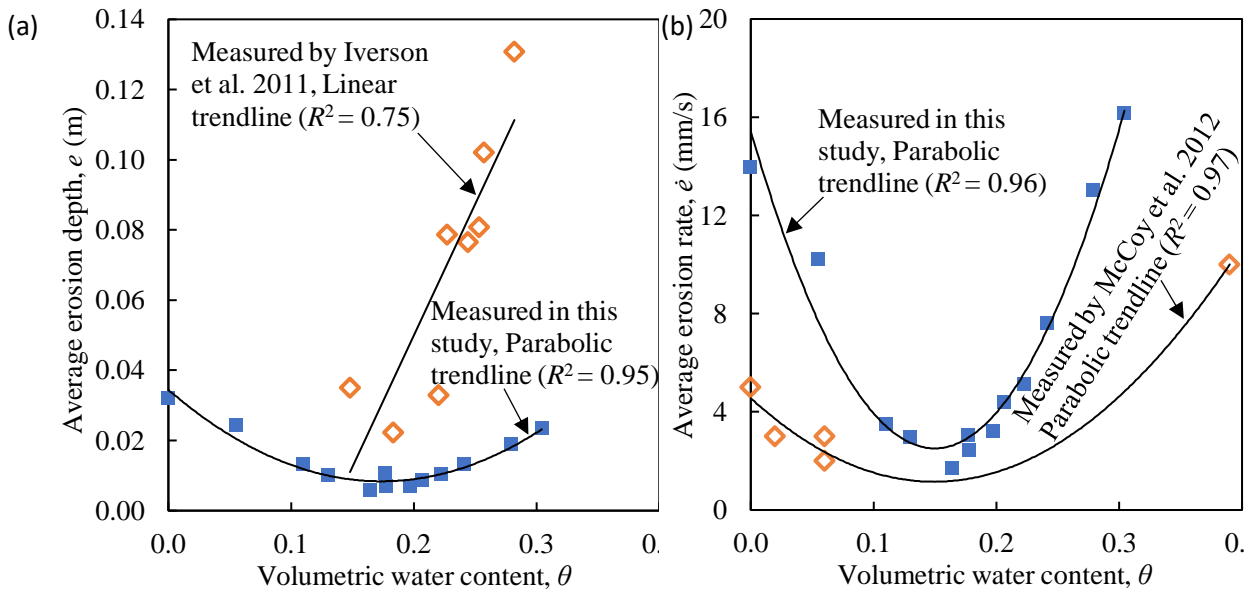


**Figure 5:** Effects of volumetric water content of the erodible bed  $\vartheta$  on erosion: (a) variation of the measured average erosion depth  $e$ ; (b) variation of measured average erosion rate  $\dot{e}$ .

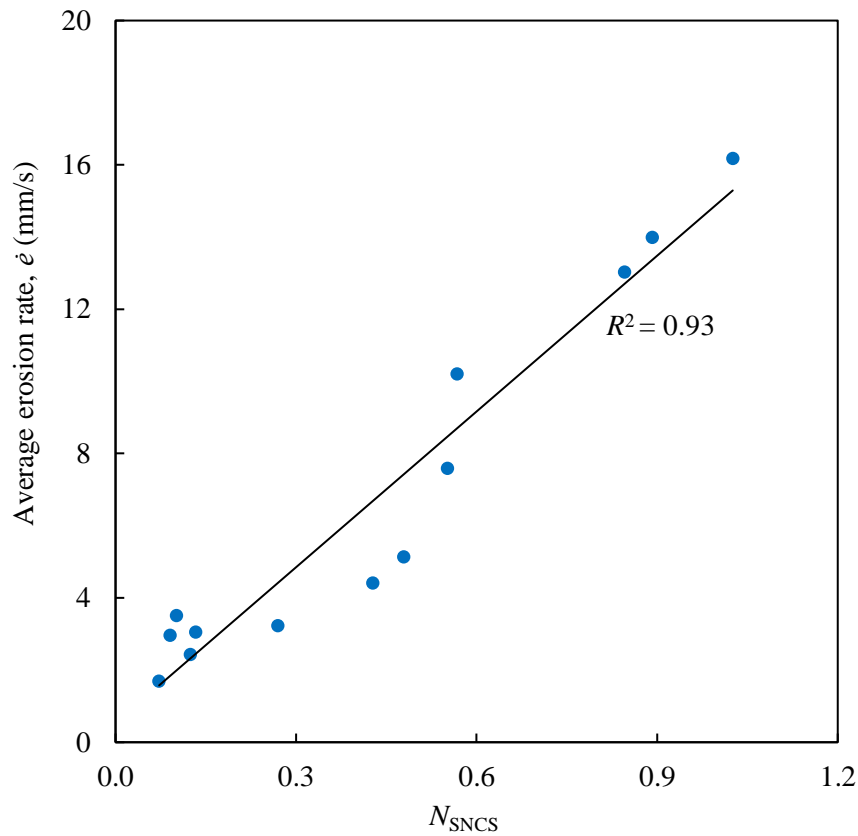


**Figure 6:** Erosion rate  $\dot{e}$  against the strength normalized collisional stress  $N_{SNCS}$ .

### 4.3 Evaluation of the $N_{SNCS}$

The strength normalized collisional stress  $N_{SNCS}$  can be calculated using Equation 8b with the necessary parameters obtained from the experiments. The experimental erosion data exhibits a positive linear correlation between the average erosion rate and  $N_{SNCS}$  (Fig. 6). This trend shows that the erosion of a soil bed is strongly influenced by the collisional stresses at the base of the flow. In the flume experiments carried out in this study, the maximum basal friction induced shear stress is estimated to be 1.4 kPa based on a flow depth of 0.1 m, which is the maximum flow depth obtained from all the experiments. Even though the shear strengths of the soil beds, with water contents from 0.11 to 0.20, are larger than the estimated maximum shear stress induced by the flow, erosion still occurs. Therefore, traditional erosion theories may need to be supplemented by the proposed collision-induced erosion theory to enhance erosion predictions. Another interesting observation supporting the notion that collisional stresses play a dominant role during erosion is that the dispersed fronts observed from the high-speed imagery do not have enduring contacts among grains, so the shear stress imposed on the soil bed can be assumed to be negligible. Yet, the soil bed is still eroded.

Similar evidence supporting the notion of collision-induced erosion can also be found in the field measurements reported by Berger et al. (2011) at Illgraben, Switzerland. For the debris flow that occurred on the 1<sup>st</sup> of July 2008, the basal normal stress, pore water pressure and basal shear stress were measured by the force plate and reported to be 35 kPa, 2 kPa and 14 kPa, respectively, when erosion was detected by the erosion sensor. If the internal friction angle of the bed material is assumed to be 34°, then the shear strength can be calculated as the product of the normal effective

stress (i.e., measured normal stress 35 kPa minus the measured pore water pressure 2 kPa) and the tangent value of the assumed friction angle (i.e.,  $34^\circ$ ). The shear strength calculated is approximately 22 kPa, which is still larger than the measured basal shear stress. This simple back-of-the-envelope calculation shows that aside from basal friction-induced shear stress, there undoubtedly should be other stresses (i.e. collisional stresses) contributing to the erosion of the soil bed. Another observation that supports the importance of collisional stresses on soil bed erosion is that the basal shear stress measured by the force plate remains relatively stable during the entire flow process (Berger et al. 2011). However, erosion predominantly occurs during the passage of the flow front, where the most collisional stresses were reported (McArdell et al. 2007).

## 5 Discussion and Conclusions

The findings from this study demonstrate the importance of hydro-mechanical coupling for delineating debris flow hazards. This is evident from the measured parabola-like relationship between water content and erosion, which is a stark contrast from the notion that erosion increases linearly with the bed water content as demonstrated by Iverson et al. (2011). There are of course many questions that remained unanswered from this conclusion alone. For instance, it appears that modelling of debris flow erosion is even more complicated of a problem than initially thought. Erosion not only depends on both the dynamic properties of the flow and the water content of the soil bed in a highly non-linear manner. Further compounding the challenges of modelling this problem are the effects of three-dimensional channel geometries and the non-uniform spatial distribution of bed water content that may occur in the field (i.e., higher water content along the centerline than further up the banks). A clear and indirect outcome from this study is that there is a pressing need to couple the hydrological and mechanical effects of soil behavior to advance the current state of debris flow modelling and hazard assessment. More importantly, soil-atmospheric interaction is very much relevant to debris flow hazard mitigation. Given the importance of capillary effects, the question that remained unanswered are how the competing effects between rainfall and humidity, driven by climate change, govern the strength of soil beds and their susceptibility to erosion? Answering these questions will help to advance the current state of landslide growth modelling and prediction.

Based on the unique field observation data (Berger et al. 2011) and the findings from this study, the theory of collision-induced erosion can help to explain the deficiencies of theories relying on purely basal friction-induced erosion. The theory of collision-induced erosion can explain why most erosion occurs mainly during the passage of the flow front (Berger et al. 2011; McCoy et al. 2012), which typically consists of highly-collisional boulders. In contrast, insignificant erosion occurs during the passage of the flow body and tail (Berger et al. 2011; McCoy et al. 2012), which have low concentrations of large boulders, and thus, weak collisional stresses. Therefore, highly erosive debris flows may develop in channels that are enriched with boulders. It is acknowledged that collisional stresses may not be the sole mechanism that drives erosion, but collisional stresses are important and often overlooked. Perhaps, models that can capture the spatial variation of collisional stresses would yield even more realistic erosion volumes and rates compared to the existing models. These considerations are required to advance debris flow predictions and delineations.

## 6 Acknowledgements

The author would also like to thank Mr. Song Pengjia for his role in advancing the research about erosion and his help to prepare this plenary paper, and Dr, Du Jianting for vetting the manuscript. The author would like to thank the Geotechnical Division Committee of the Hong Kong Institution of Engineers and the International Society for Soil Mechanics and Geotechnical Engineer for the Bright Spark Lecture Award. The author would like to express his gratitude to his colleagues in the Department of Civil Engineering at the University of Hong Kong, and his former colleagues and mentor Prof. Charles W.W. Ng from the Hong Kong University of Science and Technology for their support. Finally, the author would like to acknowledge the support provided by the Department of Civil Engineering and Faculty of Engineering at the University of Hong Kong for their support provided by the startup fund, and the support from the Research Grants Council of Hong Kong, particularly the funding from the General Research Fund (16212618; 16210219), the Early Career Scheme (27205320), and the Areas of Excellence (AoE/E-603/18).

## References

- [1] Bagnold, R.A. 1954. Experiments on a gravity-free dispersion of large solid spheres in a Newtonian fluid under shear. *Proceedings of the Royal Society of London. Series A. Mathematical and Physical Sciences*, 225(1160): 49-63.
- [2] Berger, C., McArdeell, B.W. & Schlunegger, F. 2011. Direct measurement of channel erosion by debris flows, Illgraben, Switzerland. *Journal of Geophysical Research: Earth Surface*, 116: F01002.
- [3] Bishop, A.W. 1954. The use of pore-pressure coefficients in practice. *Geotechnique*, 4(4): 148-152.
- [4] Cao, Z., Pender, G., Wallis, S. & Carling, P. 2004. Computational dam-break hydraulics over erodible sediment bed. *Journal of Hydraulic Engineering*, 130(7): 689-703.
- [5] Chen, H. & Lee, C.J. 2004. Geohazards of slope mass movement and its prevention in Hong Kong. *Engineering Geology*, 76(1-2): 3-25.
- [6] Faug, T. 2015. Macroscopic force experienced by extended objects in granular flows over a very broad Froude-number range. *The European Physical Journal E*, 38(5): 1-10.
- [7] Fraccarollo, L. & Capart, H. 2002. Riemann wave description of erosional dam-break flows. *Journal of Fluid Mechanics*, 461: 183-228.
- [8] Fredlund, D.G., Morgenstern, N.R. & Widger, R.A. 1978. The Shear-Strength of Unsaturated Soils. *Canadian Geotechnical Journal*, 15(3): 313-321.
- [9] Fredlund, D.G., Xing, A.Q., Fredlund, M.D. & Barbour, S.L. 1996. The relationship of the unsaturated soil shear strength to the soil-water characteristic curve. *Canadian Geotechnical Journal*, 33(3): 440-448.
- [10] Froude, M.J. & Petley, D.N. 2018. Global fatal landslide occurrence from 2004 to 2016. *Natural Hazards and Earth System Sciences*, 18(8): 2161-2181.
- [11] Hasan, J.U. & Fredlund, D.G. 1980. Pore pressure parameters for unsaturated soils. *Canadian Geotechnical Journal*, 17(3): 395-404.
- [12] Hilf, J. 1948. Estimating construction pore pressures in rolled earth dams. *2nd International Conference on Soil Mechanics and Foundation Engineering*, Rotterdam, Netherlands.
- [13] Hungr, O., Leroueil, S. & Picarelli, L. 2014. The Varnes classification of landslide types, an update. *Landslide*, 11(2): 167-194.
- [14] Hungr, O., McDougall, S. & Bovis, M. 2005. *Debris-flow hazards and related phenomena*. Heidelberg, Berlin: Springer.
- [15] Iverson, R.M. 1997. The physics of debris flows. *Reviews of Geophysics*, 35(3): 245-296.

- 
- [16] Iverson, R.M. 2012. Elementary theory of bed-sediment entrainment by debris flows and avalanches. *Journal of Geophysical Research: Earth Surface*, 117: F03006.
- [17] Iverson, R.M. 2015. Scaling and design of landslide and debris-flow experiments. *Geomorphology*, 244: 9-20.
- [18] Iverson, R.M., Reid, M.E., Logan, M., LaHusen, R.G., Godt, J.W. & Griswold, J.P. 2011. Positive feedback and momentum growth during debris-flow entrainment of wet bed sediment. *Nature Geoscience*, 4: 116–121.
- [19] Jaeger, J.C., Cook, N.G. & Zimmerman, R. 2009. *Fundamentals of rock mechanics*. New York: John Wiley & Sons.
- [20] Jakob, M., Stein, D. & Ulmi, M. 2012. Vulnerability of buildings to debris flow impact. *Natural Hazards*, 60(2): 241-261.
- [21] Lu, N. 2008. Is matric suction a stress variable? *Journal of Geotechnical and Geoenvironmental Engineering*, 134(7): 899-905.
- [22] McArdell, B.W., Bartelt, P. & Kowalski, J. 2007. Field observations of basal forces and fluid pore pressure in a debris flow. *Geophysical Research Letters*, 34(7): L07406.
- [23] McCoy, S.W., Kean, J.W., Coe, J.A., Tucker, G.E., Staley, D.M. & Wasklewicz, T.A. 2012. Sediment entrainment by debris flows: In situ measurements from the headwaters of a steep catchment. *Journal of Geophysical Research: Earth Surface*, 117: F03016.
- [24] McDougall, S. & Hungr, O. 2005. Dynamic modelling of entrainment in rapid landslides. *Canadian Geotechnical Journal*, 42(5): 1437-1448.
- [25] Medina, V., Hürlimann, M. & Bateman, A. 2008. Application of FLAT Model, a 2D finite volume code, to debris flows in the northeastern part of the Iberian Peninsula. *Landslides*, 5(1): 127-142.
- [26] NILIM (National Institute for Land and Infrastructure Management) 2007. Manual of technical standards for designing sabo facilities against debris flow and Driftwood, *Technical Note of NILIM No. 365. Tsukuba, Japan: Natural Institute for Land and Infrastructure Management, Ministry of Land, Infrastructure and Transport* (in Japanese).
- [27] Okuda, S., Okunishi, K. & Suwa, H. 1980. Observation of debris flow at Kamikamihori Valley of Mt. Yakedade. *3rd Meeting of IGU Commission on Field Experiment in Geomorphology*, Kyoto, Japan.
- [28] Pirulli, M. & Pastor, M. 2012. Numerical study on the erosion of bed material into rapid landslides. *Geotechnique*, 62(11): 959-972.
- [29] Savage, S.B. & Hutter, K. 1989. The motion of a finite mass of granular material down a rough incline. *Journal of Fluid Mechanics*, 199: 177-215.
- [30] Skempton, A.W. 1954. The pore-pressure coefficients A and B. *Geotechnique*, 4(4): 143-147.
- [31] Song, P. & Choi, C.E. 2021. Revealing the importance of capillary and collisional stresses on soil bed erosion induced by debris flows. *Journal of Geophysical Research: Earth Surface*. (accepted).
- [32] Sovilla, B., Burlando, P. & Bartelt, P. 2006. Field experiments and numerical modeling of mass entrainment in snow avalanches. *Journal of Geophysical Research: Earth Surface*, 111: F03007.
- [33] Stansby, P.K., Chegini, A. & Barnes, T.C.D. 1998. The initial stages of dam-break flow. *Journal of Fluid Mechanics*, 374: 407-424.
- [33] Stock, J.D. & Dietrich, W.E. 2006. Erosion of steepland valleys by debris flows. *Geological Society of America Bulletin*, 118(9-10): 1125-1148.
- [34] Sutherland, A.J. 1967. Proposed mechanism for sediment entrainment by turbulent flows. *Journal of Geophysical Research*, 72(24): 6183-6194.
- [35] Takahashi, T. 1978. Mechanical characteristics of debris flow. *Journal of the Hydraulics Division*, 104(8): 1153-1169.
- [36] Terzaghi, K.V. 1936. The shearing resistance of saturated soils and the angle between the planes of shear. *1st International Conference on Soil Mechanics*, Harvard University, US.
-

- [37] Thielicke, W. & Stamhuis, E.J. 2014. PIVlab – Towards User-friendly, Affordable and Accurate Digital Particle Image Velocimetry in MATLAB. *Journal of Open Research Software*, 2(1): e30.
- [38] Vanapalli, S.K., Fredlund, D.G., Pufahl, D.E. & Clifton, A.W. 1996. Model for the prediction of shear strength with respect to soil suction. *Canadian Geotechnical Journal*, 33(3): 379-392.